Towards ultrathin Pt films on nanofibres by surface-limited electrodeposition for electrocatalytic applications

Giorgio Ercolano, Filippo Farina, Sara Cavaliere, Deborah J. Jones, Jacques Rozière

Towards ultrathin Pt films on nanofibres by surface-limited electrodeposition for electrocatalytic applications

Giorgio Ercolano, Filippo Farina, Sara Cavaliere*, Deborah J. Jones and Jacques Rozière

Novel fuel cell nanofibrous electrodes (NFEs) with higher degree of platinum exploitation and higher durability compared to commercial standards are produced, based on self-standing electrospun carbon nanofiber webs covered by platinum ultrathin nanoislands deposited by high overpotential pulsed electrodeposition.

Introduction

Reduction of the fabrication costs and improved durability are the key to a successful market penetration of proton exchange membrane fuel cells (PEMFC).[1] Platinum is at the centre of oxygen reduction reaction (ORR) electrocatalyst production and research. A more effective and durable utilization of this rare and highly priced metal is paramount to the development of a less expensive and more appealing PEMFC.[2–4] The platinum resource being limited, a substantial reduction of its use will offer a key advantage for the success of a sustainable energy technology. One limitation of Pt nanoparticles is that ORR activity is related to the size, low coordination sites and the inevitable presence of less active crystalline planes[5]. Furthermore, the nature of nanoparticles generates a limited carbon-platinum interface and a tendency to migration and agglomeration during duty cycles as a consequence of electrochemical Ostwald ripening.[1,6–8]

The deposition of extended Pt surfaces as, for example, in the nanostructured thin film (NSTF) approach developed by 3M[9], has been shown to produce 10 fold higher surface activity than nanoparticles and better durability than those of conventional carbon-supported nanoparticles. This class of electrocatalysts introduces novel and promising features at the expense of a significantly more complex fabrication process. It opened a new field of research dedicated to thin metal film on various type of support. The percolating/continuous nature of the Pt films reduces the support function to mechanical scaffolding. The extended support-metal interface of the NSTFs has reduced ohmic losses when compared to the high carbon/nanoparticles contact resistance typical of limited interfaces. Their continuous conformal morphology minimises unused platinum *e.g.* the contribution from coordinatively unsaturated sites including edges and corners of conventional Pt nanoparticulate catalysts.[10] As a consequence, higher ORR specific activity is achieved compared to nanoparticle-based electrodes.[9,11–14] Furthermore, the stability of the Pt thin film based electrodes is enhanced due to the protective effect of the metal layer on the support and the lower tendency of extended surfaces to electrochemical Ostwald ripening.[15–17] Despite these clear advantages, the complexity of the fabrication process used to generate high Pt specific surface area in films is limiting their adoption.[18–21] The challenge in depositing and controlling conformal morphology and film thickness out of the line of sight on high aspect ratio supports has led to investigation of the potential of gas phase atomic layer deposition[18,22,23], Cu underpotential deposition-redox replacement[19,21], spontaneous galvanic displacement[24] and plasma-assisted deposition.[20] Alloying of Pt with transition metals,[25,26] or the de-alloying of PtM (M = transition metal);[27,28] is another powerful strategy used to improve ORR performance.

Here we present a novel class of electrocatalysts that consists of Pt conformally electrodeposited around the carbon surface of a self-standing nanofibrous electrode (NFE). We found that combining two cost-effective and up-scalable techniques, electrospinning and electrodeposition, it is possible to obtain an electrocatalyst with outstanding Pt exploitation and high durability while minimizing fabrication complexity. We produced hierarchical 3D electrocatalyst layers with tuneable morphology that could be analysed directly and potentially used as such in a MEA (membrane electrode assembly), allowing the complete exploitation of their highly porous structure, in a

similar fashion to NSTF or other 3D macroscopic assembly techniques.[29–31] These structured electrocatalyst layers have high electrical conductivity for fast charge transport, and diffused macroporosity for efficient reactant mass transportation.[32]

Experimental

Polyacrylonitrile (PAN, Mw=150,000, Sigma Aldrich) derived carbon fibres were prepared following electrospinning with thermal treatments as already reported.[33–36] In detail 8 % (w/w) PAN solution in N,N-dimethylformamide (DMF, 98 %, Sigma Aldrich) was fed to a metal needle via a syringe pump with a flow rate of 1 ml/h. An electric field of 15 kV was applied between the needle and a metallic rotating drum collector (Spraybase) placed at a distance of 10 cm. As-prepared PAN fibres were collected in the form of non-woven mats. Fibre carbonization was realized by a two-step thermal treatment. First oxidative stabilization was performed at 280 °C for 1 h followed by carbonization for 1 h under N_2 at 1500 °C using a heating ramp of 4 °C/min. The resulting carbon electrodes were subsequently treated at 80 °C in 5 M HNO_3 solution for 5 hr.

Electrical conductivity was measured using a 2400 Keithley in a 4 wire configuration on a 5 x 40 x 0.05 mm carbon electrode strip in a Fumatech MK3-L cell operated in the current range 0-100 mA.

The ultimate tensile strength was measured in an Instron 5544 on a 25 x 5 x 0.05 mm carbon strip elongated at 0.1 mm/min.

Pt electrodeposition was performed in a 2-electrode setup, where the counter electrode consisted of a 20 x 50 x 0.8 mm graphite foil facing the working electrode and kept 10 mm away; the latter was a 15 x 40 x 0.05 mm carbon nanofibre self-standing mat. Both electrodes were dipped in a N_2 saturated 0.1 M H_2PtCl_6 $5H_2O$ solution and contacted using Pt wires. The deposition voltage was alternated between -3.0 V and 0.0 V for the desired number of pulses and duration. Samples were thoroughly washed with deionized water (18 MΩ cm), dried and weighed on a microbalance.

Thermogravimetric analysis was performed in air up to 800 °C (10 °C/min) using a Netzsch STA 409PC thermobalance to determine Pt loading on the diverse carbonaceous supports.

The morphology of the electrospun materials and of the deposited Pt was analysed by field emission-scanning electron microscopy (FE-SEM) using a Hitachi S-4800 microscope and by transmission electron microscopy (TEM) using a JEOL 2200FS (Source: FEG) microscope operating at 200 kV equipped with a CCD camera Gatan USC (16 MP). For TEM analyses, samples were suspended in ethanol and sonicated before deposition onto carbon-coated copper grids. The average diameter and density of Pt structures were determined by measuring 100 selected objects using the ImageJ software.

Powder X-ray diffraction (XRD) patterns were recorded at room temperature in Bragg-Brentano configuration using a PANAlytical X'pert diffractometer, equipped with a hybrid monochromator, operating with CuK_α radiation (λ = 1.541 Å), and using a step size of 0.05° 2θ within the 2θ domain from 20 to 70 °.

Electrochemical analyses were carried out in a three-electrode cell comprising a glassy carbon rotating disk electrode (RDE) (working electrode geometric area 0.196 cm^2), a reversible hydrogen electrode (RHE, reference electrode) and a platinum wire (counter electrode), and a BioLogic SP300 potentiostat. All the potential values are referred to the RHE.

As a conventional reference, 5 mg of 57 wt.% Pt/C (HiSPEC 9100 from Johnson Matthey) were mixed with 1 mL of DI water, 4 mL of ethanol (Aldrich) and 35 µL of the 5 wt.% Nafion® solution in alcohols (Aldrich). After 20 min of sonication, 7 µl of ink was deposited onto the electrodes and dried for 10 min to obtain a total Pt loading of 4 µg on the RDE tip.

For the electrodeposited Pt, disk (φ = 4 mm) shaped self-standing electrodes were cut from electrodeposited samples using a punch tool and attached to the glassy carbon RDE tip.

Electrochemical measurements were performed in a 0.1 M $HClO_4$ solution saturated with either N_2 or O_2. In particular ECSA determination was performed by CV in N_2 saturated 0.1 M $HClO_4$ cycling between 0.05 and 1.2 V (vs RHE) at a scan rate of 5 mV/s, while linear sweep voltammetry was performed in O_2 saturated 0.1 M $HClO_4$ between 0.2 and 1.2 V (vs RHE) at a scan rate of 20 mV/s and RDE rotating speed 1600 RPM. Cyclic voltammetry based accelerated degradation was performed by cycling between 0.6 and 1.2 V at 500 mV/s for 10,000 cycles measuring the ECSA every 100th cycle at 20 mV/s.

Results and discussion

Carbon nanofibrous electrodes are prepared from polyacrilonitrile (PAN) derived electrospun carbon nanofibres, and have been demonstrated to be a potentially viable alternative carbon support for electrocatalysts.[37–43] We achieved fine control over electrode thickness, nanofibre diameter, degree of orientation and hydrophilicity.[39,43]

Mechanical properties (ultimate tensile strength 2.2 MPa, similar to other inorganic electrospun self-standing mats[44]) and electrical conductivity (σ = 32 S cm^{-1}, Figure S1) of the prepared electrodes are more than adequate to perform electrodeposition.

Due to poor nucleation, standard electrodeposition has been shown to produce large (50 – 200 nm) and sparse Pt aggregates. Furthermore, diffusion of the noble metal through the porous electrode quickly becomes the limiting factor, generating inhomogeneous deposition.[40,45,46] Self-limited layer-by-layer electrodeposition of thin platinum group metal films has been reported on gold and nickel substrates.[47–49] This method could not be transposed as such on the electrodes in this work due to the different nature of the substrates both in terms of their surface chemistry, morphology and more importantly electrodynamic behaviour, but it provided an advantageous starting point for the outcomes in this work.

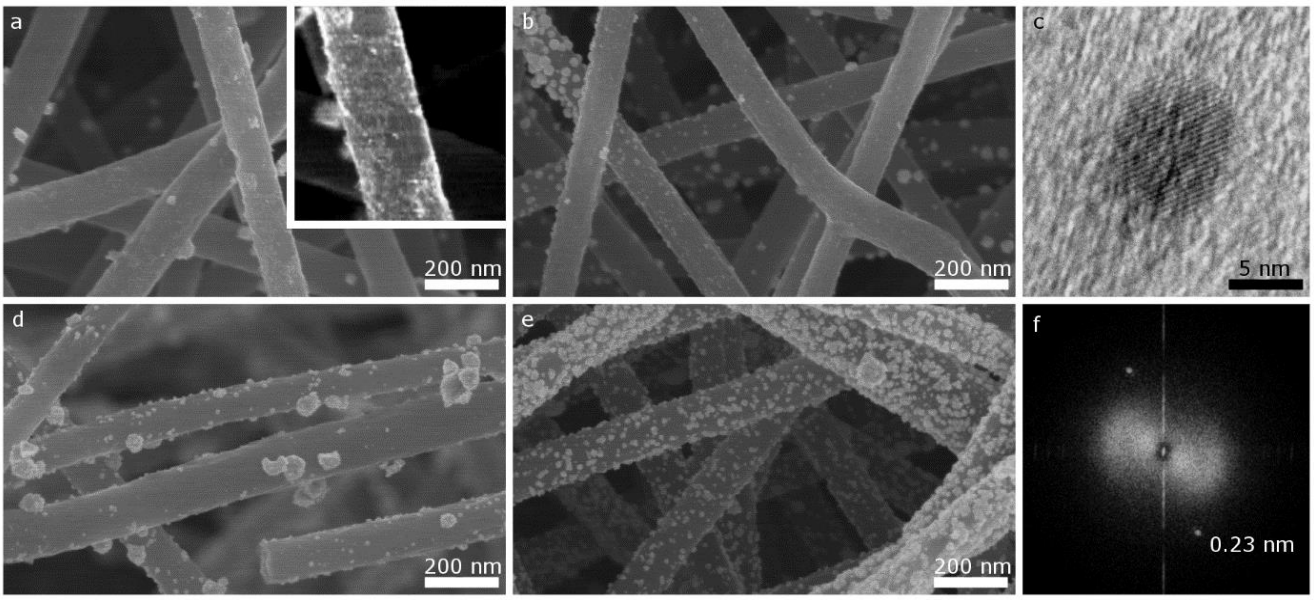

Figure 1. SEM micrographs of NFE deposited with various pulses times. 1 pulse of 200 s internal (a) and external layers (b) of the electrodes, 5 pulses of 40 sec internal (d) and external layers (e) of the electrodes, (c) HRTEM micrographs of an isolated Pt nanoplatelet and (f) the respective FFT images.

A pulsed electrodeposition obtained by alternating the voltage between a small overpotential to the Pt deposition in the hydrogen evolution region on Pt (-1.0 V *vs* SCE for 1 minute) and a resting potential (+0.4 V *vs* SCE for 2 minutes) as suggested for self-limited Pt deposition methods on metal surfaces[47], while improving nucleation did not improve homogeneity nor produced thin smooth Pt films. To evaluate the Pt deposition dynamics we prepared a set of NFE using a higher overpotential to improve nucleation [50–53] (-3.0 V and 0.0 V in a two electrode setup). All

samples shared the same total deposition time of 200 s, which was divided into a different number of pulses. Pt loading values were measured by thermogravimetric analysis (TGA) to calculate the Pt deposition rate during a single pulse: the calculated Pt deposition rate is typical for diffusion limited processes and shows a sharp decay during the first 10 seconds of a pulse, after which a severely diffusion limited constant deposition rate is reached (Figure S2). This sharp decay is consistent with an increase mass transfer overpotential induced by an increasingly thicker boundary layer generated by the reactant consumption. The combined effect of pulse duration and number of pulses over the morphology of the deposited Pt was investigated by electron microscopies.

The morphology obtained is strongly dependent on the pulse time range: only pulses ≥ 40 s produce a morphology approaching the targeted Pt extended surface, being composed of a mosaic of flat nanoplatets on the carbon fibre and only few large nanoparticles (>20 nm); with shorter pulses (from 20 to 1 second), a dense distribution of large Pt aggregates is produced (Figure S3), indicating that efficient nucleation requires longer pulse times.[9]

The morphology of Pt surfaces obtained with long pulses (200-40 sec) was investigated by scanning electron microscopy. Two-dimensional nanoplatelets all over the fibre surface were distinguishable, as a metal "background" (inset in Figure 1a). HRTEM allowed their observation (Figure 1c) (their crystallinity was further demonstrated by XRD, Figure S4) as well as the determination of their exposed crystal facets (Figure 1f), the (111) (d = 0.23 nm), which are known to have higher initial ORR specific activity than the (100). [54–56] From the electrochemical surface area measurements, we can estimate a thickness lower than 1 nm for these platelets (see later in the text). Similar two-dimensional objects with a plate-like morphology and thickness of 1.3-1.6 nm were obtained under similar conditions by electrodeposition on Highly Oriented Pyrolytic Graphite (HOPG).[57] In order to better observe the morphology features of the NFE, we increased the deposited Pt amount onto the carbon mats by increasing the number of pulses (while keeping the total deposition time fixed at 200 s). The SEM observations were performed both on the inner and outer layers of the electrodes to investigate the homogeneity of the platinum deposition (Figure 1). Inhomogeneity of Pt growth occurs as the number of pulses increases. A detailed analysis of the formation and morphology of large Pt aggregates formed on increasing the number of pulses, and its effect on the electrochemical properties can be found in the Electronic Supplementary Information (Figure S5 and S6). Indeed, for 1 pulse of 200 s the Pt dispersion appears quite homogenous all over the electrode thickness, while for 5 pulses of 40 s, preferential growth onto existing nanoislands occurs at the external surface of the electrode (thus in direct contact with the electrodeposition solution), while less Pt is deposited in the inner part of the NFE. The experimentally observed higher Pt deposition rate on the NFE external layer compared to the inner layer is typical in diffusion-limited depositions[58] and is in agreement with the calculated Pt deposition rate typical of diffusion limited processes (Figure S2).

Furthermore, this phenomenon can be intensified by the strong hydrogen evolution occurring at the high overpotentials imposed. Indeed, gas evolution can promote mass transfer to the external layers reducing the diffusion layer thickness and effectively increasing the deposition rate to these areas.[53] In addition, ohmic effects could also contribute to the deposition gradient, yet the relevance of the two controlling factors cannot be quantified. As expected, increasing the pulse number amplifies the observed difference (Figure S3). We can thus observe Pt growth on existing nanoplatelets, which ultimately leads to a thick continuous layer on the outer part of the electrode beyond 10 electrodeposition cycles.

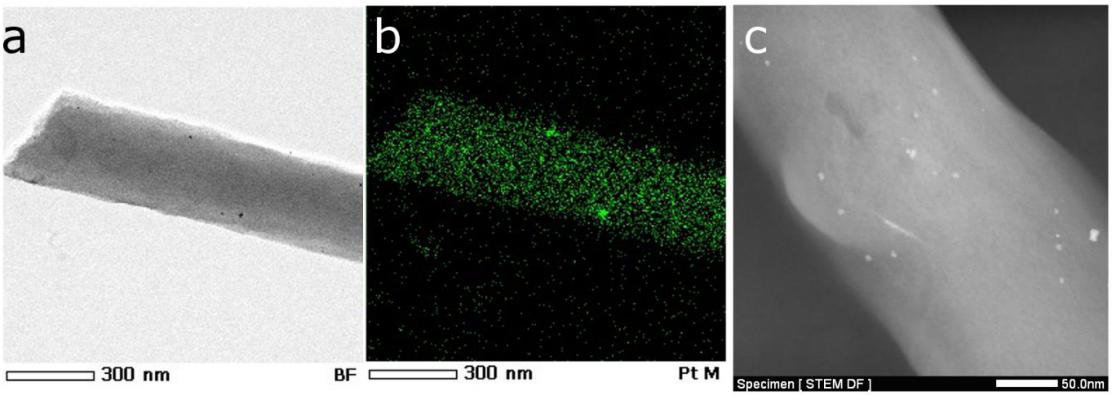

Figure 2. STEM micrographs of platinum covered nanofibres: Bright field (a) and relative platinum EDX map (b). (c) HAADF STEM image.

The existence of an ultrathin diffuse platinum coverage is confirmed by the STEM images taken on fibres with a minimum amount of platinum agglomeration obtained with a 200 s deposition time. In particular the EDX map in Figure 2b provides evidence for the presence of platinum in regions where no particles are visible in the bright field STEM of Figure 2a. In addition, HAADF (Figure 3c) also suggests a diffuse almost complete coverage of platinum showing only slightly darker regions where bare carbon is exposed. An ultrathin diffuse coverage was obtained using the same deposition protocol on a model HOPG surface and observed by AFM, providing additional support for the above conclusions. Electrochemical properties were evaluated directly on disk shaped electrodes mechanically attached on a glassy carbon RDE tip (Figure 3a). Extremely high Pt exploitation was observed: the electrochemical specific surface area (ECSA) was calculated from the hydrogen adsorption charges.[59] ECSA exceeding 120 m^2g^{-1} was measured for the sample prepared with a 40 sec pulse; this value is comparable to those obtained in electrocatalysts with Pt nanoparticles with diameter in the range 1-2 nm.[60,61]. Similar values were obtained with the sample deposited with a single 200 s pulse (ECSA ~ 140 m^2g^{-1}). These values are smaller than the theoretical value for a (111) oriented Pt monolayer (265 m^2g^{-1}) yet higher than those expected for a continuous Pt film (around 60 $m^{2\ -1}$ for a 1 nm thick film), and it is due to the presence of discrete nano-platelets. This also indicates that the Pt utilisation is much higher when Pt is synthesized directly on the fibre surface provided that the agglomeration is kept to a minimum and the dispersion is maximized. The ECSA of ca. 140 m^2g^{-1} was used to derive an indirect indication of the platelet thickness of < 1 nm. It is thus evident that the presence of the few large nanoparticles on the fibre surface (Figure 1a and d) has little influence on the overall ECSA values.

All the prepared NFE are active towards the oxygen reduction reaction (ORR). Figure 3b is an example of a typical ORR curve taken at 1600 RPM in oxygen saturated 0.1 M $HClO_4$ solution (the NFE shown was prepared with 40 s pulses). ORR onset potential reaches 1.07 V_{RHE} and at 0.9 V_{RHE} (the typical reference potential at which compare electrocatalytic activities) the reaction is already into the diffusion-limited domain. Due the thickness of the support (~ 50 µm) and the mounting setup it is impossible to calculate reliable mass activity values without modelling the oxygen diffusion through a thick layer and taking into consideration the presence of a limiting kinetic current after the external diffusion effect is corrected.[62] Nevertheless, without considering that the mounting setup (Figure S7) partially masks the electrode from the electrolyte and disturbs a normal laminar flow, and without taking into account the oxygen diffusion through the thick layer, a value of 130 A g^{-1} at 0.9 V_{RHE} was calculated for the mass activity of the NFE. This mass activity is vastly underestimated due to the impossibility of applying the adequate corrections to the measured currents. Tafel slopes of ~70 mV $decade^{-1}$ confirm a 4 electron pathway.

A second key factor, as essential as Pt exploitation, is the stability of the catalyst over time. Support corrosion together with Pt dissolution, migration and agglomeration tend to reduce the available electroactive surface. The samples were aged by cycling the potential between 0.6 V and 1.2 V in the range of both carbon and platinum degradation, and the change in ECSA was monitored to evaluate the stability of the catalysts (Figure 3d).

ECSA decay was lower for the NFE (-39 %) compared to the commercial electrocatalyst (-55 %). After 10,000 potential cycles, the ECSA of the aged NFEs (77 m^2g^{-1}) is still comparable to that of fresh (non-aged) conventional Pt/C (78 m^2g^{-1}). These values are even higher than those obtained when using highly corrosion resistant metal oxide supports that however, present lower electrocatalytic performance.[35,63–65] Furthermore, the ECSA decay trend of conventional Pt/C is identical to that of carbon nanofibres also bearing Pt nanoparticulate catalysts and submitted to the same accelerated stress test: [66] in both cases only 45 % of ECSA is retained after 10,000 electrochemical cycles. This result demonstrates that combination of Pt morphology and deposition method seems to be more crucial than the morphology of the support itself. Therefore the nature of the Pt/support interface and the presence of thin 2D Pt islands are key factors to explain the increased stability. Electrodeposited Pt tends to form an extended interface with the support that increases the adhesion and the amount of carbon that needs to be removed before a particle is free to migrate; thus increasing the stability of the system. This result is further confirmed by ORR activity evaluation after accelerated stress testing. Figure 3b shows that at the halfway point the total loss was around 10 mV for the NFE and 58 mV for conventional Pt/C.

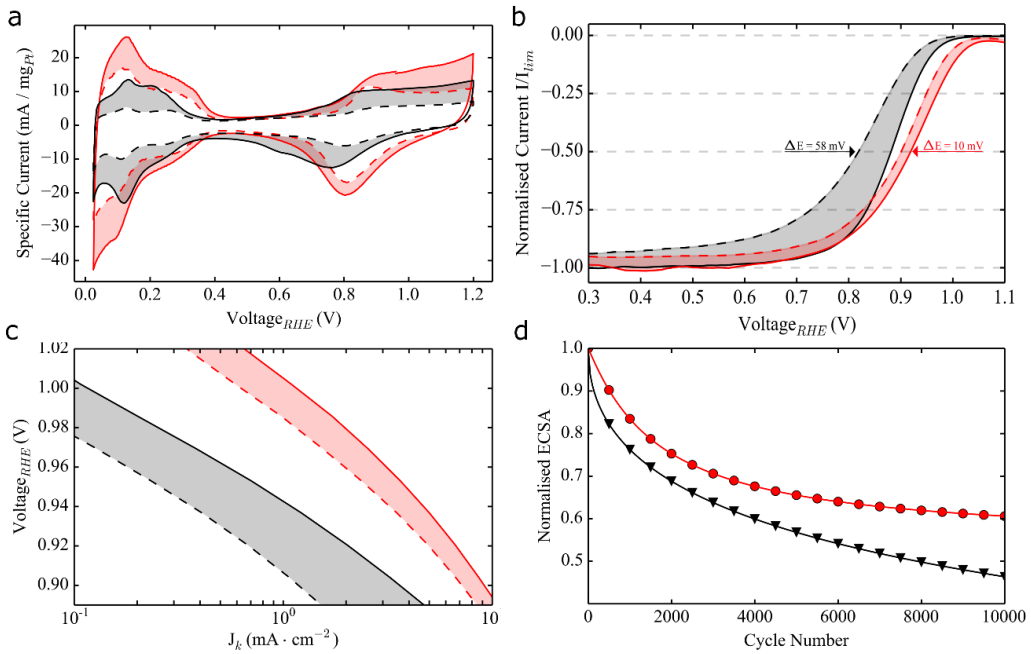

Figure 3. (a) Cyclic voltammetry in N_2 saturated 0.1 M $HClO_4$, (b) oxygen reduction reaction polarisation curves at 1600 RPM and (c) the corresponding Tafel analysis. (d) Normalised electrochemically active surface area as a function of the number of voltage cycles. The samples compared are conventional Pt/C in black, 40 s pulse in red.

Whilst the *ex situ* characterisation of the NFE produced is overwhelmingly promising, performance of these electrodes in devices such as fuel cells, where oxygen reduction occurs at or near the 3-phase (electrode surface, electrolyte, gas phase) boundary, may be significantly different, and may not necessarily directly translate to high performance.

The requirements for a good electrocatalyst layer include high gas/ion transport to and from the catalyst: the thickness, low geometric surface areas and anisotropic connectivity of the NFE will have to be addressed to achieve the full potential in MEA operation. We are now pursuing various approaches to adapt the characteristics of the above NFEs to fuel cell MEA application.

Conclusions

We demonstrated that it is possible to produce highly stable and hierarchically structured 3 dimensional nanofibrous electrodes (NFEs) with outstanding Pt exploitation and electrochemical stability combining two simple and cost-effective techniques: electrospinning and electrodeposition. In particular we showed how controlling the pulse length in a pulsed Pt electrodeposition can be used to obtain extended metal surfaces composed of nanoislands on self-standing nanofibrous carbon mats. The ECSA of these novel electrocatalysts reaches 140 m^2g^{-1}, higher than that of most highly optimised currently available commercial catalysts. This new class of catalysts intermediate between NTSF and conventional carbon black supported Pt nanoparticles shows outstanding stability, significantly higher than what is achieved with conventional methods and without the introduction of more stable but less conductive metal oxide supports. Support morphology does not define alone the stability of the electrocatalyst, it is paramount to maximise support interface with the Pt catalyst.

High ECSA, durability over time of the prepared catalyst layer combined with the scalability of the adopted process makes NFEs prime candidates as alternative to conventional Pt/C catalysts, as well as to NTSF and Pt/metal oxides or carbides.

Acknowledgements

The research leading to these results has received funding from the European Research Council (ERC) under the European Union's Seventh Framework Programme (FP/2007-2013) / ERC Grant Agreement SPINAM n. 306682.

Funding from the European Community's Seventh Framework Programme (FP7/2013-2016) for the Fuel Cells and Hydrogen Joint Technology Initiative under grant agreement CATAPULT n. 325268 is also acknowledged.

Notes and references

1 R. Borup, J. Meyers, B. Pivovar, Y. S. Kim, R. Mukundan, N. Garland, D. Myers, M. Wilson, F. Garzon, D. Wood, P. Zelenay, K. More, K. Stroh, T. Zawodzinski, J. Boncella, J. E. McGrath, M. Inaba, K. Miyatake, M. Hori, K. Ota, Z. Ogumi, S. Miyata, A. Nishikata, Z. Siroma, Y. Uchimoto, K. Yasuda, K.-I. Kimijima and N. Iwashita, *Chem. Rev.*, 2007, **107**, 3904–3951.

2 L. Su, W. Jia, C.-M. Li and Y. Lei, *ChemSusChem*, 2014, **7**, 361–78.

3 R. R. Adzic, J. Zhang, K. Sasaki, M. B. Vukmirovic, M. Shao, J. X. Wang, A. U. Nilekar, M. Mavrikakis, J. a. Valerio and F. Uribe, *Top. Catal.*, 2007, **46**, 249–262.

4 R. R. Adzic, *Electrocatalysis*, 2012, **3**, 163–169.

5 H. Lv, D. Li, D. Strmcnik, A. P. Paulikas, N. M. Markovic and V. R. Stamenkovic, *Nano Energy*, 2016, 1–17.

6 S. Zhang, X.-Z. Yuan, J. N. C. Hin, H. Wang, K. A. Friedrich and M. Schulze, *J. Power Sources*, 2009, **194**, 588–600.

7 A. Taniguchi, T. Akita, K. Yasuda and Y. Miyazaki, *J. Power Sources*, 2004, **130**, 42–49.

8 K. Hartl, M. Hanzlik and M. Arenz, *Energy Environ. Sci.*, 2011, **4**, 234–238.

9 E.E. Parsonage and M.K. Debe, US5338430 A, 1994.

10 S. M. Alia, Y. Yan and B. Pivovar, *Catal. Sci. Technol.*, 2014, **4**, 3589–3600.

11 N. Kristian and X. Wang, *Electrochem. commun.*, 2008, **10**, 12–15.

12 S. M. Alia, S. Pylypenko, K. C. Neyerlin, D. a. Cullen, S. S. Kocha and B. S. Pivovar, *ACS Catal.*, 2014, **4**, 2680–2686.

13 A. B. Papandrew, R. W. Atkinson, G. A. Goenaga, D. L. Wilson, S. S. Kocha, K. C. Neyerlin, J. W. Zack, B. S. Pivovar and T. A. Zawodzinski, *ECS Trans.*, 2013, **50**, 1397–1403.

14 S. S. Kocha, J. W. Zack, S. M. Alia, K. C. Neyerlin and B. S. Pivovar, *ECS Trans.*, 2013, **50**, 1475–1485.

15 M. K. Debe, *Nature*, 2012, **486**, 43–51.

16 M. K. Debe, A. K. Schmoeckel, G. D. Vernstrom and R. Atanasoski, *J. Power Sources*, 2006, **161**, 1002–1011.

17 I. E. L. Stephens, A. S. Bondarenko, U. Grønbjerg, J. Rossmeisl and I. Chorkendorff, *Energy Environ. Sci.*, 2012, **5**, 6744.

18 Q. Du, J. Wu and H. Yang, *ACS Catal.*, 2014, **4**, 144–151.

19 M. Khosravi and M. K. Amini, *Int. J. Hydrogen Energy*, 2010, **35**, 10527–10538.

20 E. Dilonardo, A. Milella, P. Cosma, R. d'Agostino and F. Palumbo, *Plasma Process. Polym.*, 2011, **8**, 452–458.

21 Y.-G. Kim, J. Y. Kim, D. Vairavapandian and J. L. Stickney, *J. Phys. Chem. B*, 2006, **110**, 17998–8006.

22 N. P. Dasgupta, C. Liu, S. Andrews, F. B. Prinz and P. Yang, 2013.

23 A. A. Dameron, S. Pylypenko, J. B. Bult, K. C. Neyerlin, C. Engtrakul, C. Bochert, G. J. Leong, S. L. Frisco, L. Simpson, H. N. Dinh and B. Pivovar, *Appl. Surf. Sci.*, 2012, **258**, 5212–5221.

24 S. M. Alia, Y. S. Yan and B. S. Pivovar, *Catal. Sci. Technol.*, 2014, **4**, 3589–3600.

25 V. R. Stamenkovic, B. S. Mun, M. Arenz, K. J. J. Mayrhofer, C. A. Lucas, G. Wang, P. N. Ross and N. M. Markovic, *Nat. Mater.*, 2007, **6**, 241–247.

26 V. R. Stamenkovic, B. Fowler, B. S. Mun, G. Wang, P. N. Ross, C. A. Lucas and N. M. Marković, *Science*, 2007, **315**, 493–7.

27 S. Koh and P. Strasser, *J. Am. Chem. Soc.*, 2007, **129**, 12624–12625.

28 P. Strasser and S. Kühl, *Nano Energy*, 2016.

29 S. Chen, J. Duan, M. Jaroniec and S.-Z. Qiao, *Adv. Mater.*, 2014, **26**, 2925–30.

30 S. Chen, J. Duan, M. Jaroniec and S. Z. Qiao, *Angew. Chem. Int. Ed. Engl.*, 2013, **52**, 13567–70.

31 H. J. Qiu, Y. Ito, W. Cong, Y. Tan, P. Liu, A. Hirata, T. Fujita, Z. Tang and M. Chen, *Angew. Chemie - Int. Ed.*, 2015, **54**, 14031–14035.

32 Y. Zheng, Y. Jiao and S. Z. Qiao, *Adv. Mater.*, 2015, **27**, 5372–8.

33 C.-K. Liu, K. Lai, W. Liu, M. Yao and R.-J. Sun, *Polym. Int.*, 2009, **58**, 1341–1349.

34 N. Yusof and A. F. Ismail, *J. Anal. Appl. Pyrolysis*, 2012, **93**, 1–13.

35 I. Savych, J. Bernard d'Arbigny, S. Subianto, S. Cavaliere, D. J. Jones and J. Rozière, *J. Power Sources*, 2014, **257**, 147–155.

36 S. Cavaliere, S. Subianto, I. Savych, D. J. Jones and J. Rozière, *Energy Environ. Sci.*, 2011, **4**, 4761–4785.

37 D. Sebastián, A. G. Ruíz, I. Suelves, R. Moliner, M. J. Lázaro, V. Baglio, A. Stassi and A. S. Aricò, *Appl. Catal. B Environ.*, 2012, **115**–**116**, 269–275.

38 B. Wu, D. Hu, Y. Kuang, Y. Yu, X. Zhang and J. Chen, *Chem. Commun. (Camb).*, 2011, **47**, 5253–5255.

39 J. J.-H. Park, Y.-W. Y. Ju, S.-H. S. Park, H. H.-R. Jung, K.-S. Yang and W.-J. Lee, *J. Appl. Electrochem.*, 2009, **39**, 1229–1236.

40 Z. Lin, L. Ji and X. Zhang, *Electrochim. Acta*, 2009, **54**, 7042–7047.

41 M. Li, Y. Chang, G. Han and B. Yang, *J. Power Sources*, 2011, **196**, 7973–7978.

42 Y. Wang, J. Jin, S. Yang, G. Li and J. Qiao, *Electrochim. Acta*, 2015, **177**, 181–189.

43 E. Yli-Rantala, a. Pasanen, P. Kauranen, V. Ruiz, M. Borghei, E. Kauppinen, a. Oyarce, G. Lindbergh, C. Lagergren, M. Darab, S. Sunde, M. Thomassen, S. Ma-Andersen and E. Skou., *Fuel Cells*, 2011, **11**, 715–725.

44 Y. Wang, W. Li, Y. Xia, X. Jiao and D. Chen, *J. Mater. Chem. A*, 2014, **2**, 15124.

45 M. Li, G. Han and B. Yang, *Electrochem. commun.*, 2008, **10**, 880–883.

46 H. Kim, N. P. Subramanian and B. N. Popov, *J. Power Sources*, 2004, **138**, 14–24.

47 Y. Liu, D. Gokcen, U. Bertocci and T. P. Moffat, *Science*, 2012, **338**, 1327–30.

48 Y. Liu, C. M. Hangarter, D. Garcia and T. P. Moffat, *Surf. Sci.*, 2015, **631**, 141–154.

49 S. H. Ahn, H. Tan, M. Haensch, Y. Liu, L. A. Bendersky and T. P. Moffat, *Energy Environ. Sci.*, 2015, **8**, 3557–3562.

50 M. E. Hyde and R. G. Compton, *J. Electroanal. Chem.*, 2003, **549**, 1–12.

51 R. N. Bhattacharya, M. Feldmann, D. Larbalestier and R. D. Blaugher, in *IEEE Transactions on Applied Superconductivity*, 2001, vol. 11, pp. 3102–3105.

52 N. . Qu, D. Zhu, K. . Chan and W. . Lei, *Surf. Coatings Technol.*, 2003, **168**, 123–128.

53 N. D. Nikolić, K. I. Popov, L. J. Pavlović and M. G. Pavlović, *Surf. Coatings Technol.*, 2006, **201**, 560–566.

54 M. A. Hoque, F. M. Hassan, D. Higgins, J.-Y. Choi, M. Pritzker, S. Knights, S. Ye and Z. Chen, *Adv. Mater.*, 2015, **27**, 1229–34.

55 N. Markovic, H. Gasteiger and P. N. Ross, *J. Electrochem. Soc.*, 1997, **144**, 1591–1597.

56 D. F. van der Vliet, C. Wang, D. Tripkovic, D. Strmcnik, X. F. Zhang, M. K. Debe, R. T. Atanasoski, N. M. Markovic and V. R. Stamenkovic, *Nat. Mater.*, 2012, **11**, 1051–8.

57 I. Lee, K.-Y. Chan and D. L. Phillips, *Appl. Surf. Sci.*, 1998, **136**, 321–330.

58 Z. D. Wei, S. H. Chan, L. L. Li, H. F. Cai, Z. T. Xia and C. X. Sun, *Electrochim. Acta*, 2005, **50**, 2279–2287.

59 S. Trasatti and O. A. Petrii, *J. Electroanal. Chem.*, 1992, 327, 353–376.

60 D. Sebastián, I. Suelves, E. Pastor, R. Moliner and M. J. Lázaro, *Appl. Catal. B Environ.*, 2013, **132**, 13–21.

61 J. C. Meier, C. Galeano, I. Katsounaros, J. Witte, H. J. Bongard, A. A. Topalov, C. Baldizzone, S. Mezzavilla, F. Schüth and K. J. J. Mayrhofer, 2014, 44–67.

62 Y.-H. Shih, G. V. Sagar and S. D. Lin, *J. Phys. Chem. C*, 2008, **112**, 123–130.

63 S. Cavaliere, S. Subianto, I. Savych, M. Tillard, D. J. Jones, J. Rozière and D. J. Jones, *J. Phys. Chem. C*, 2013, **117**, 18298–18307.

64 I. Savych, S. Subianto, Y. Nabil, S. Cavaliere, D. Jones and J. Rozière, *Phys. Chem. Chem. Phys.*, 2015, **17**, 16970–16976.

65 S. Cavaliere, I. Jiménez-Morales, G. Ercolano, I. Savych, D. Jones and J. Rozière, *ChemElectroChem*, 2015, **2**, 1966–1973.

66 C. Marichy, G. Ercolano, G. Caputo, M. G. Willinger, D. Jones, J. Rozière, N. Pinna and S. Cavaliere, *J. Mater. Chem. A*, 2016, **4**, 969–975.